Supplement of Geosci. Model Dev., 19, 10479–10502, 2026
https://doi.org/10.5194/gmd-19-10479-2026-supplement
© Author(s) 2026. CC BY 4.0 License.



Geoscientific Model Development
Open Access
EGU

Supplement of

cSINGV v1.0: development and evaluation of a 1.5 km coupled atmosphere–ocean–wave modelling system for the Western Maritime Continent

Rajesh Kumar et al.

Correspondence to: Rajesh Kumar (rajesh_kumar@nea.gov.sg)

The copyright of individual parts of the supplement might differ from the article licence.

Supplement

This supplement provides additional figures and tables supporting the evaluation of the ocean and wave components, precipitation diagnostics, case studies, and air–sea flux analysis presented in the main manuscript.

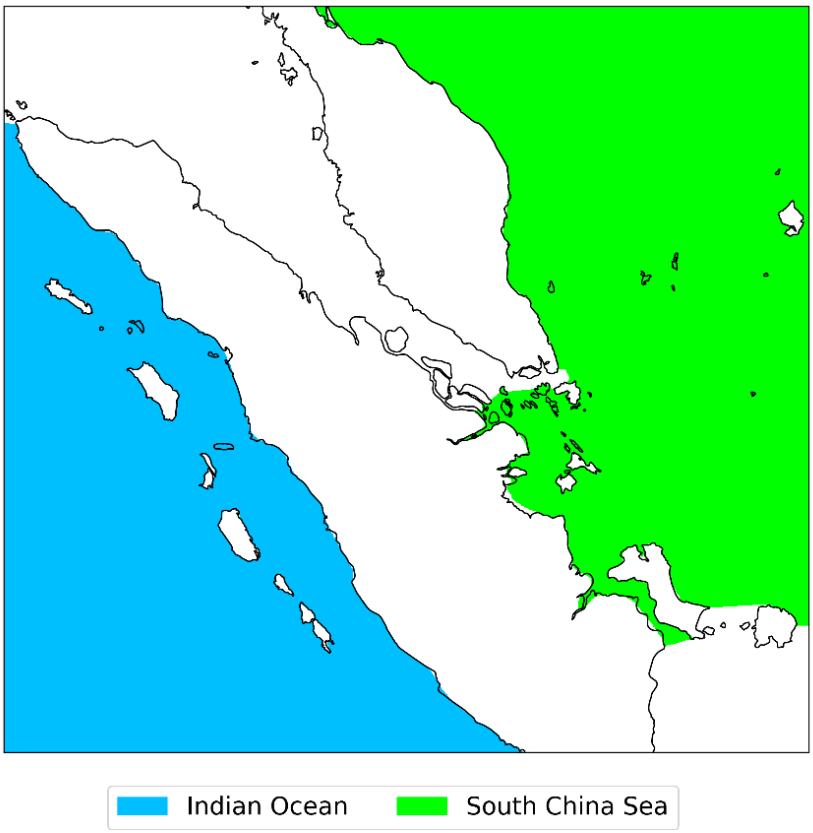


Figure S1. Model domain of the coupled atmosphere–ocean–wave system. Shaded regions indicate the subdomains used for ocean evaluation: the Indian Ocean (blue) and the South China Sea (green). These regions represent contrasting dynamical regimes used for regional analysis in Section 4.1.

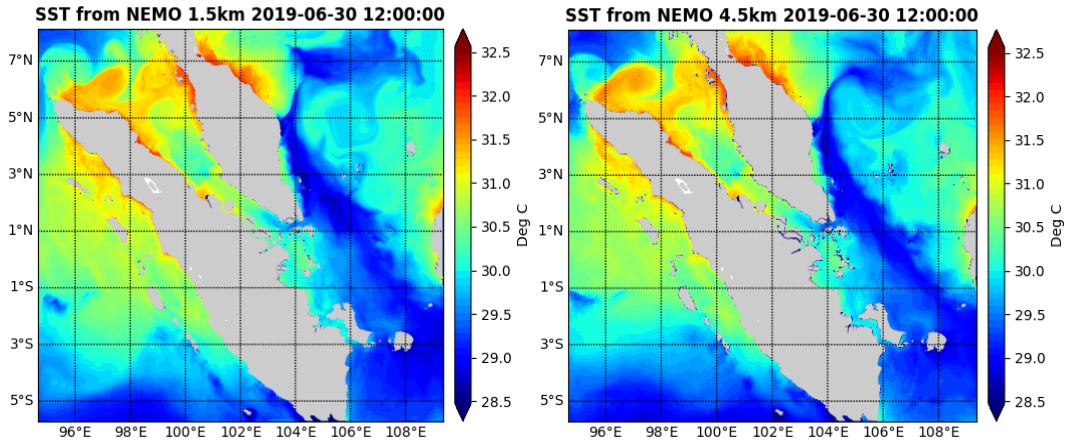


Figure S2. Comparison of the 1.5 km NEMO configuration with the prototype 4.5 km NEMO configuration (Thompson et al., 2021).

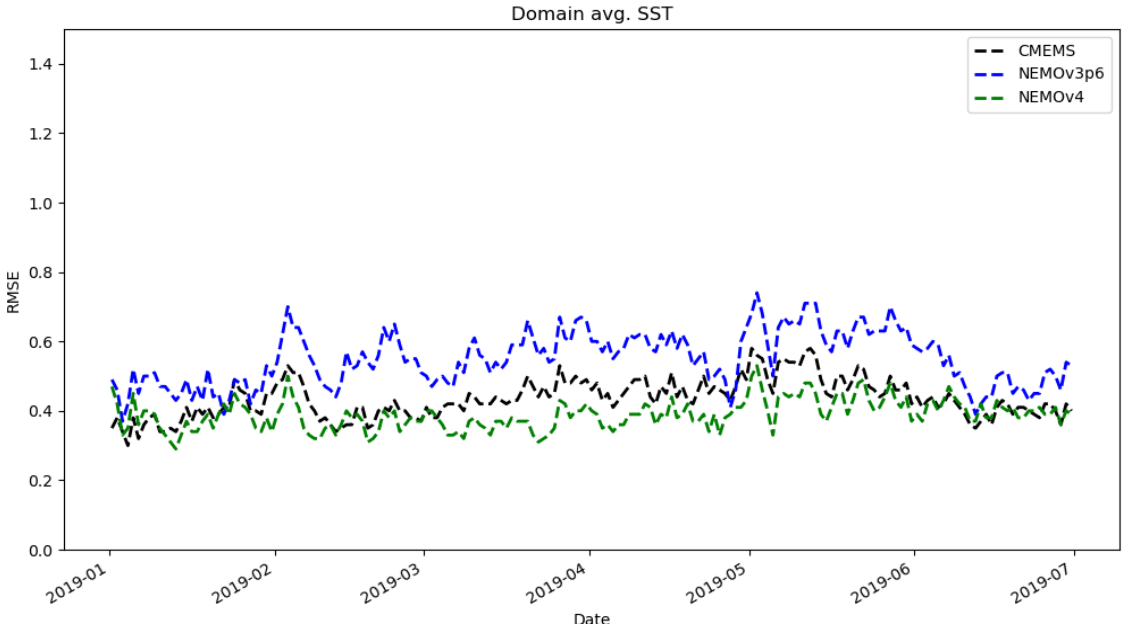


Figure S3. Time series comparison of domain-averaged SST for the 1.5 km (green dashed line) and 4.5 km (blue dashed line) NEMO configurations.

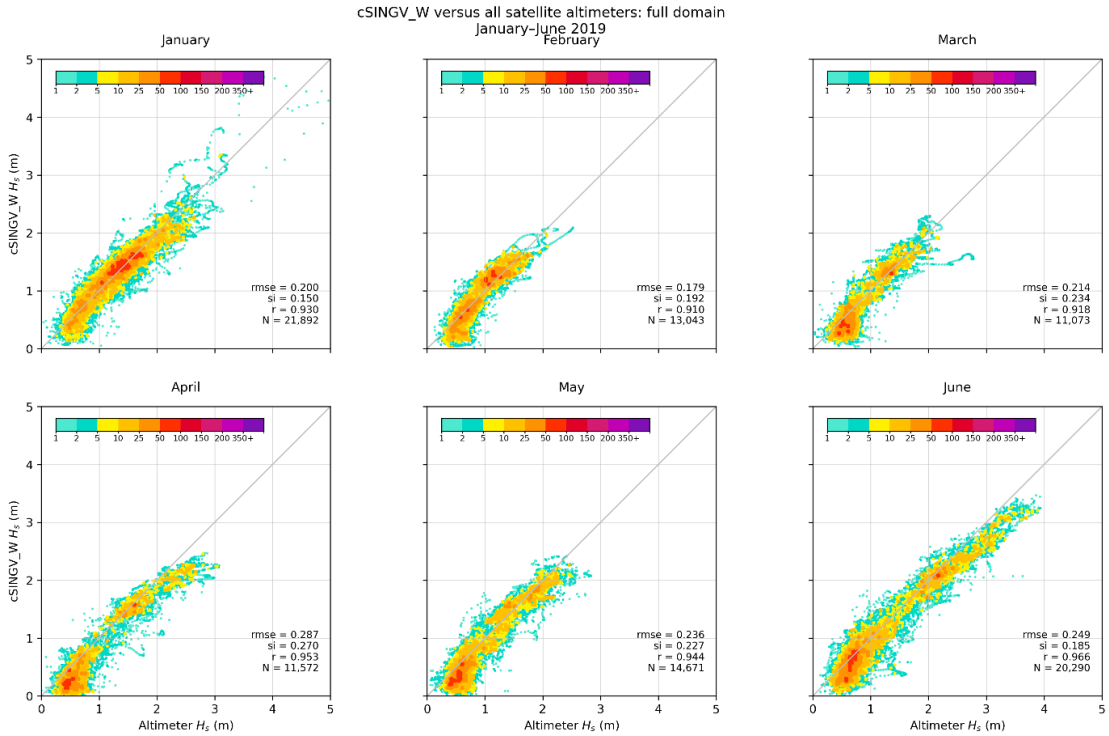


Figure S4. Monthly comparison of significant wave height (H_s) from the standalone wave simulation cSINGV_W against satellite-altimeter observations over the full model domain during January–June 2019.

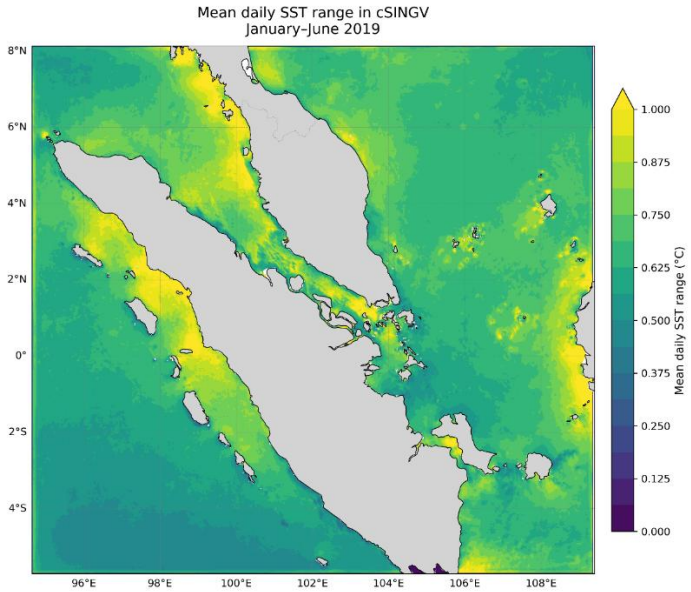


Figure S5. Mean daily sea-surface temperature (SST) range in cSINGV during January–June 2019. The daily SST range was calculated as the difference between the maximum and minimum of the 24 hourly SST values and then averaged over all available days.

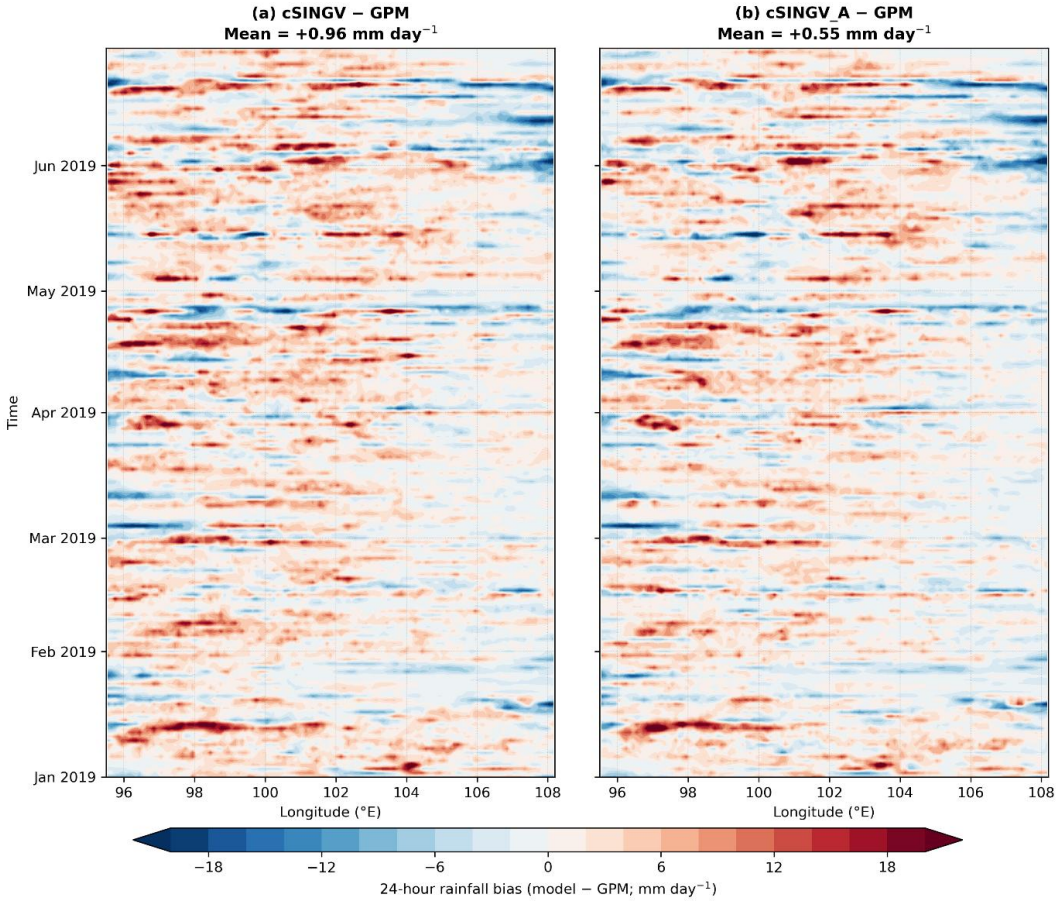


Figure S6. Longitude–time distribution of the daily precipitation bias relative to GPM averaged between 5°S and 8°N during January–June 2019 for (a) cSINGV and (b) cSINGV_A.

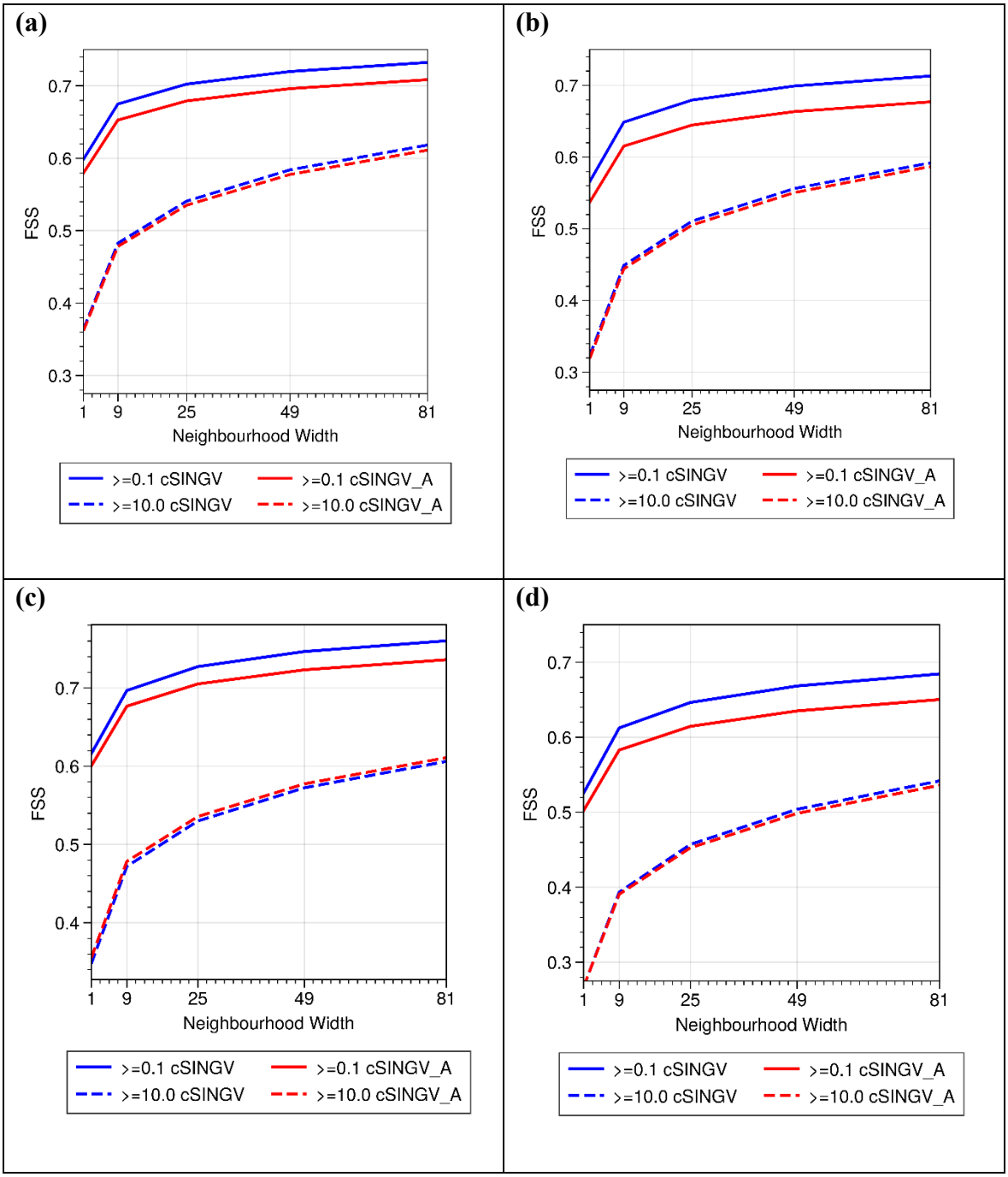


Figure S7. FSS as a function of neighbourhood width for (a) January, (b) February, (c) April, and (d) May 2019, evaluated at two precipitation thresholds: ≥0.1 mm (solid lines) and ≥10.0 mm (dashed lines). Blue lines represent the coupled model (cSINGV) simulations, while red lines represent the uncoupled model (cSINGV_A) simulations. The neighbourhood width is expressed in terms of grid cells; for example, a width of 81 corresponds to a 9 × 9 grid box, equivalent to approximately 13.5 km × 13.5 km at the model resolution of 1.5 km.

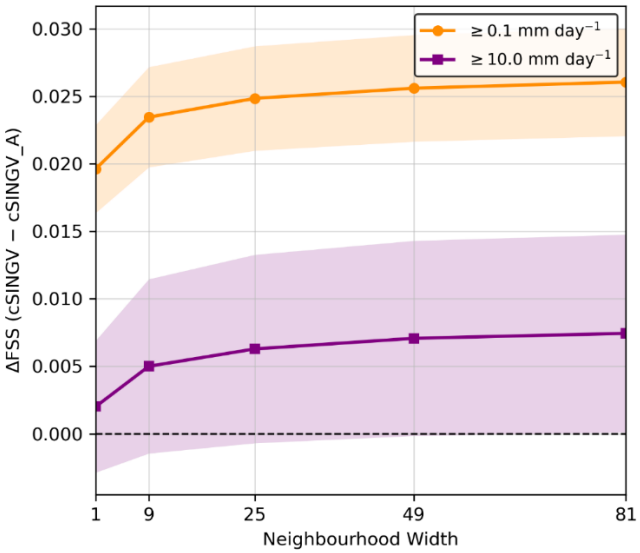


Figure S8. Mean paired difference in Fractions Skill Score (ΔFSS = cSINGV − cSINGV_A) as a function of neighbourhood width for daily precipitation thresholds of ≥0.1 and ≥10.0 mm day⁻¹ during January–June 2019. Shading indicates the 95% confidence interval calculated from the paired daily differences, and the horizontal dashed line denotes no difference.

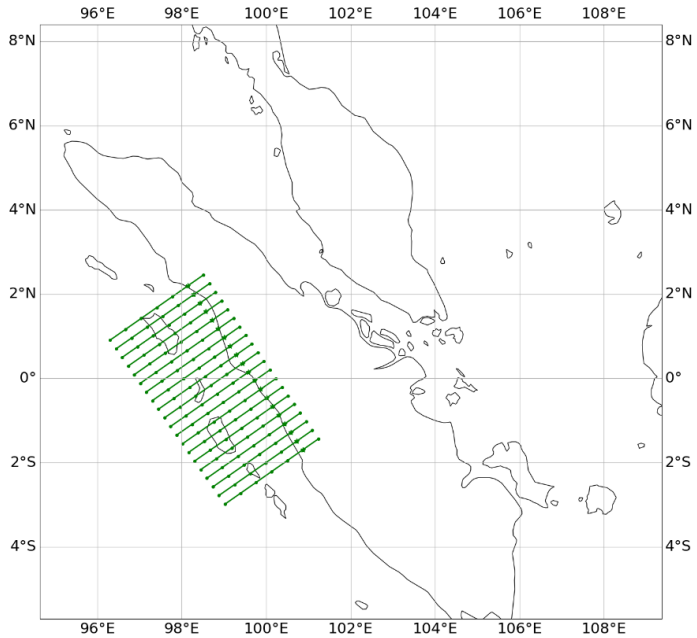


Figure S9. Location and orientation of the transects used for the Hovmöller analysis across western Sumatra. The green lines indicate a set of parallel transects oriented approximately perpendicular to the western coastline of Sumatra, extending from the Indian Ocean (offshore) toward inland regions. These transects are used to construct the diurnal rainfall Hovmöller diagrams shown in Fig. 8.

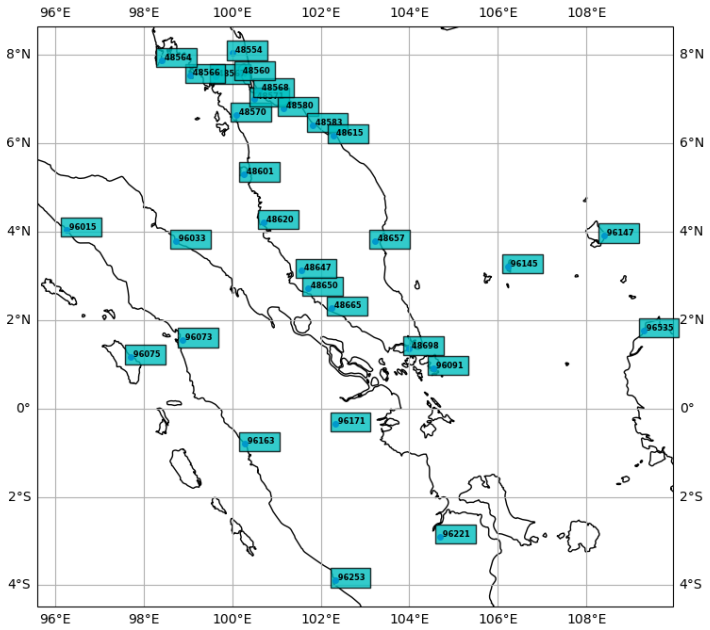


Figure S10. Location of WMO MetDB observation stations used for evaluation. Station IDs correspond to those used in the comparison of near-surface atmospheric variables.

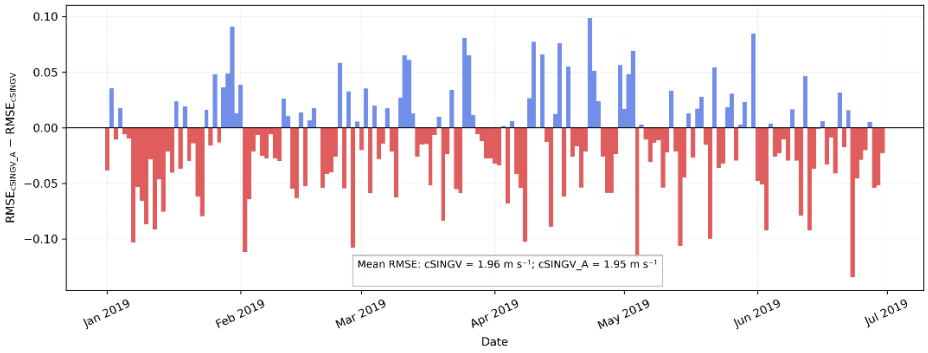


Figure S11. Daily paired differences in 10-m wind-speed RMSE (ΔRMSE = $RMSE_{cSINGV_A} - RMSE_{cSINGV}$) during January–June 2019. Positive (blue) values indicate lower RMSE in the coupled cSINGV simulation, whereas negative (red) values indicate lower RMSE in cSINGV_A.

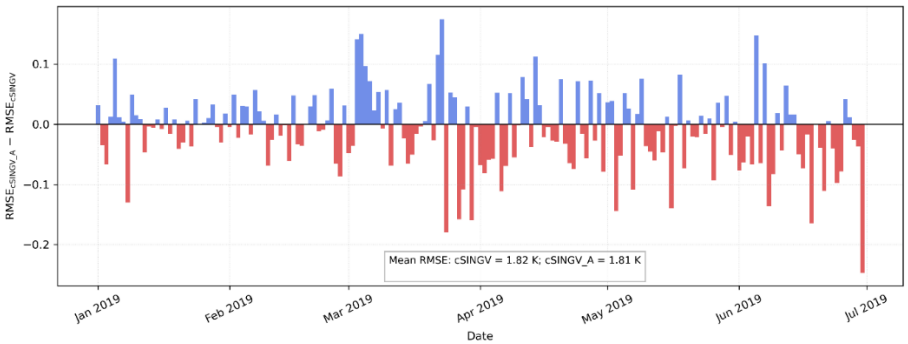


Figure S12. Same as Figure S11, but for 2 m air temperature.

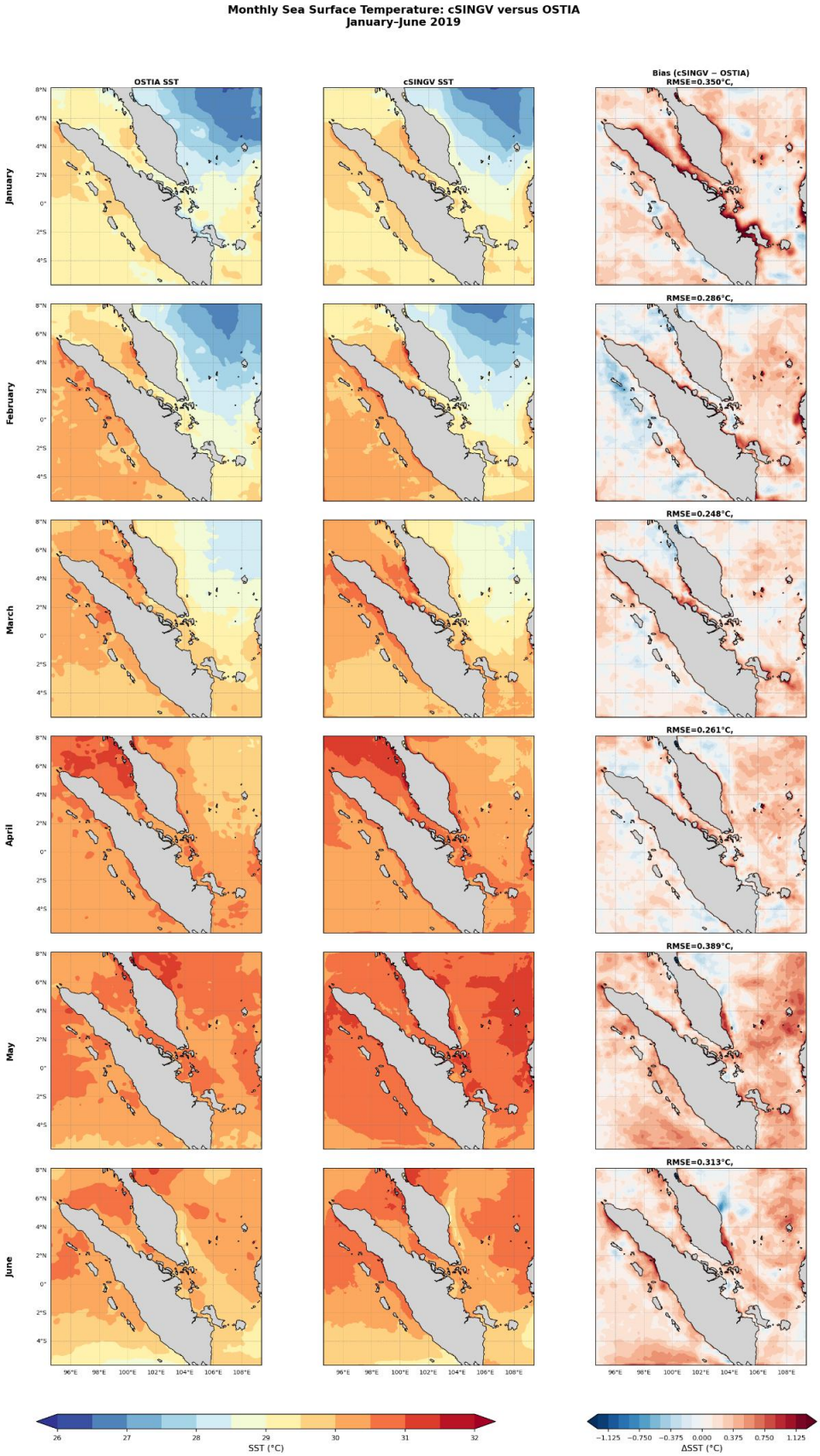


Figure S13. Monthly mean sea-surface temperature (SST) from OSTIA (left column) and the fully coupled cSINGV simulation (middle column), together with the corresponding cSINGV − OSTIA SST bias (right column), during January–June 2019.

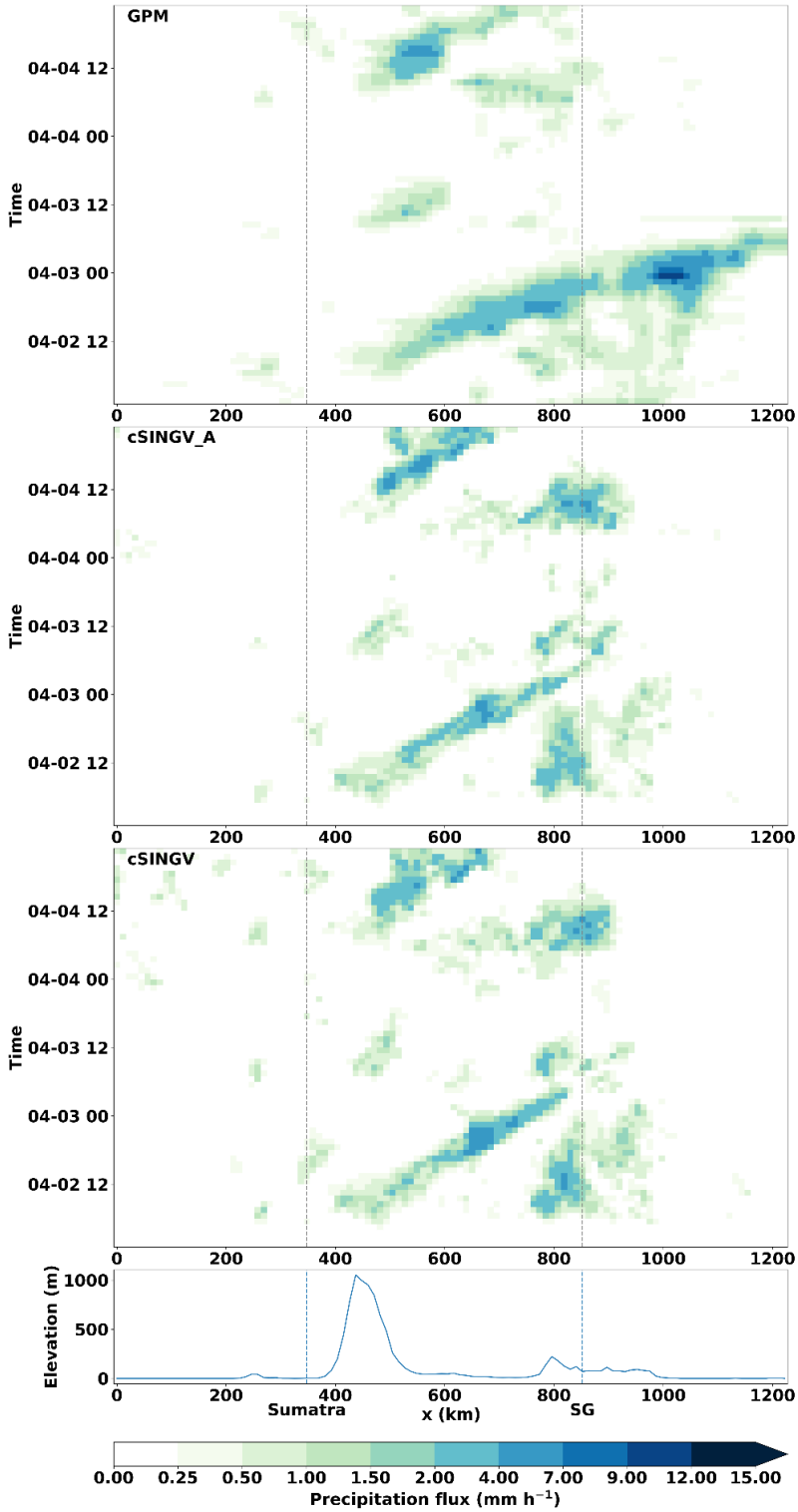


Figure S14. Rotated Hovmöller diagram of precipitation for the 2–4 April 2019 Sumatra squall event. Top: GPM observations; middle: uncoupled simulation (cSINGV_A); bottom: coupled simulation (cSINGV).

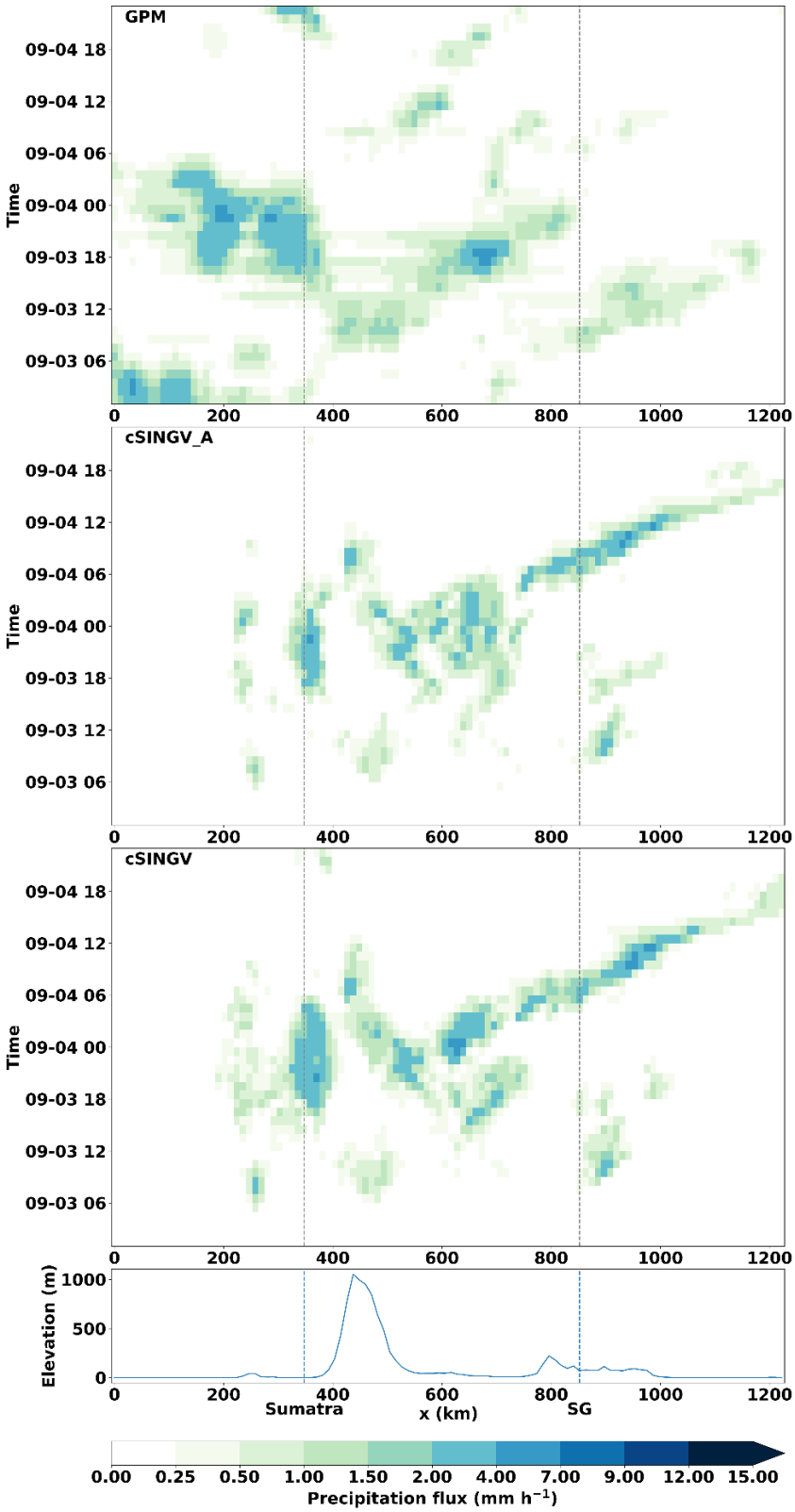


Figure S15. Same as Fig. S14, but for the 3–4 September 2019 event.

The convection exhibits a more fragmented structure during its propagation, with similar behaviour in both configurations.

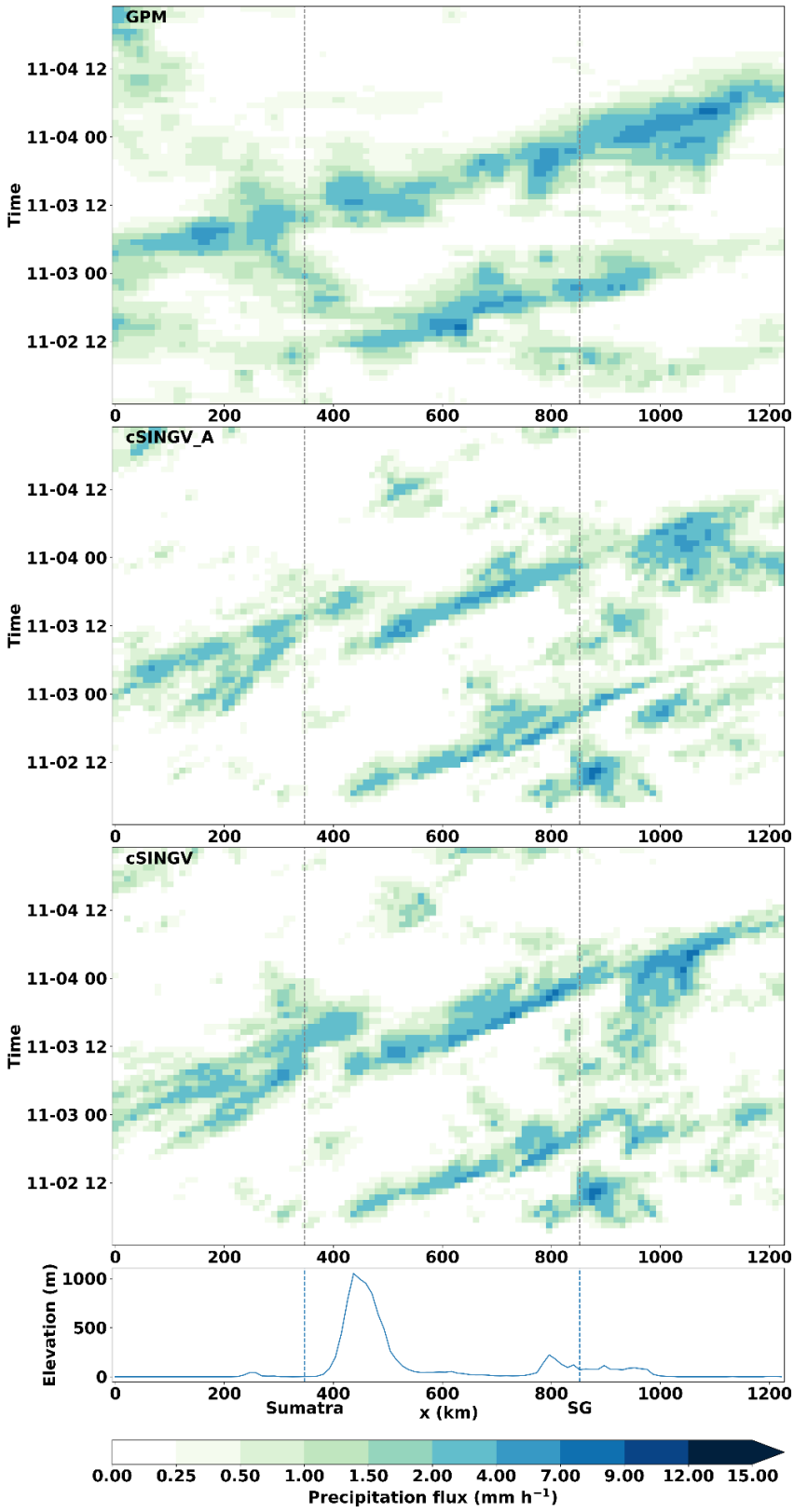


Figure S16. Same as Fig. S14, but for the 2–4 November 2020 event.

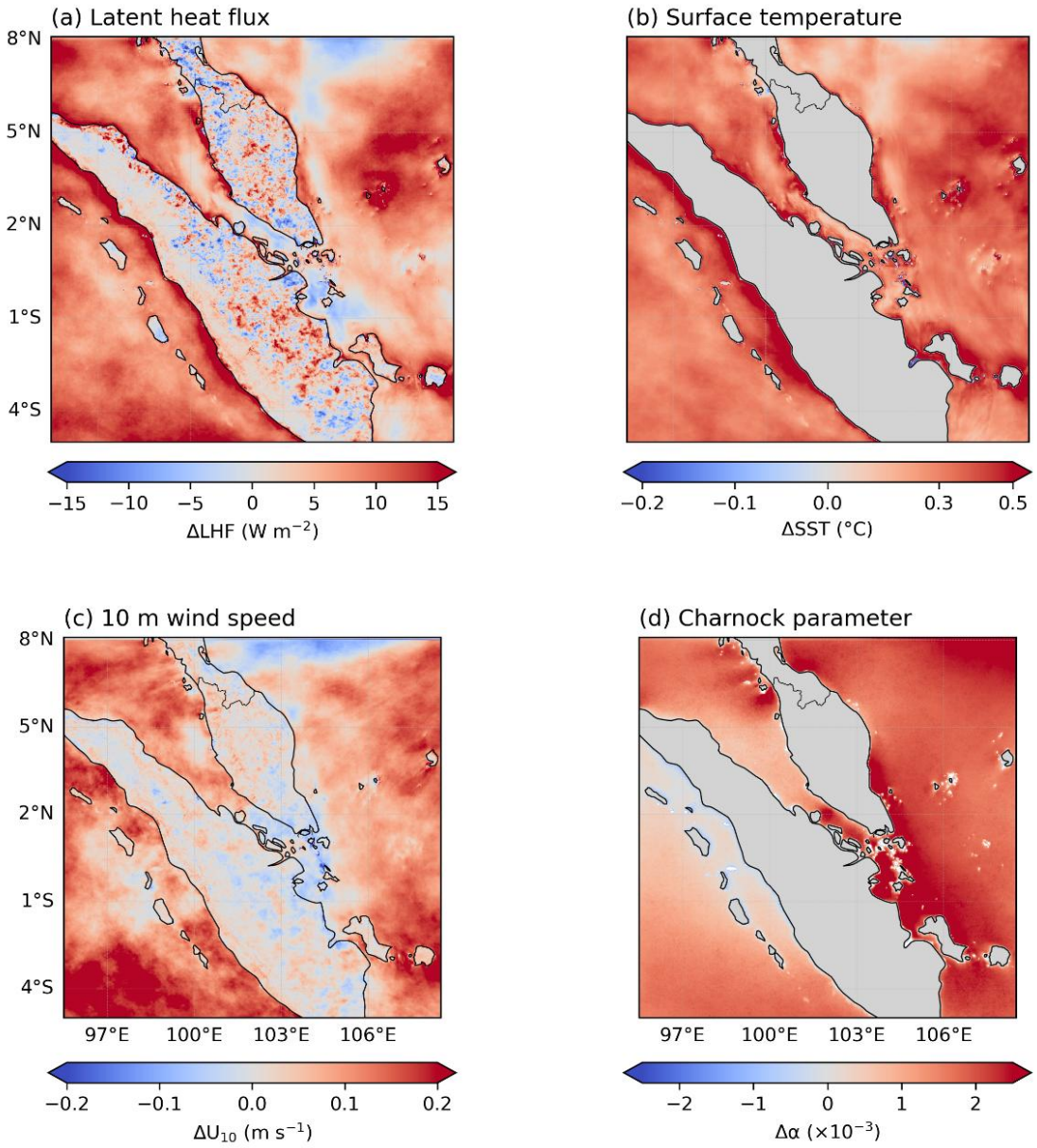


Figure S17. January–June 2019 mean differences between cSINGV and cSINGV_A (cSINGV minus cSINGV_A) in (a) latent heat flux, (b) SST, (c) 10 m wind speed and (d) Charnock parameter. The Charnock parameter difference is calculated relative to the fixed value of 0.011 used in cSINGV_A.

Table S1. Summary of namelist configuration changes applied in the upgrade from NEMO v3.6 to v4.0.4.

Namelist	NEMO v4.0.4	NEMO v3.6
nambbl	nn_bbl_ldf=1 rn_ahtbbl=1000. rn_gambbl=10.	nn_bbl_ldf=0
nambdy	ln_bdy=.true. rn_time_dmp=1. rn_time_dmp_out=1	ln_sponge=.true. rn_sponge=5
namdom	?	?
namdyn_ldf	ln_dynldf_blp=.true. ln_dynldf_lev=.true. nn_ahm_ijk_t=31 rn_ahm_b=0. rn_csmc=3.5 rn_minfac=1.0 rn_maxfac=1.0	ln_dynldf_bilap=.true. ln_dynldf_level=.true. rn_ahm_0_blp=-6.0e7 rn_ahm_m_blp=-6.0e7 rn_cmsh=1 rn_cmsmag_1=3.0 rn_cmsmag_2=3
		[namelist:namdyn_nept] ln_neptramp=.true. rn_htrmax=200.0 rn_htrmin=100.0 rn_tslse=1.2e4 rn_tslsp=3.0e3
nameos	ln_eos80=.true. rn_a0=1.6550e-1 rn_b0=7.6554e-1 rn_lambda1=5.9520e-2 rn_lambda2=7.4914e-4 rn_lambda2=7.4914e-4 rn_mu1=1.4970e-4 rn_mu2=1.1090e-5 rn_nu=2.4341e-3	
namsbc	ln_traqsr=.true.	
namsbc_blk/ namsbc_core (v3.6)	ln_coare_3p5=.true. rn_zqt=2.	rn_zqt=10
namtra_adv	ln_traadv_fct=.true	ln_traadv_tvd=.true.
namtra_ldf	ln_traldf_blp=.true. ln_traldf_lev=.true.	ln_traldf_lap=.true. ln_traldf_hor=.true.

namdyn_spg	ln_dynspg_ts=.true. ln_bt_av=.true. nn_bt_flt=1 ln_bt_auto=.true. rn_bt_cmax=0.8 nn_baro=10	
namtra_qsr	ln_qsr_rgb=.true. rn_abs=0.58 rn_si1=23.0	ln_traqsr=.true. ln_qsr_rgb=.true. rn_abs=0.56 !!rn_si1=20.0
namtrd	ln_tra_trd=.true.	ln_tra_trd=.false.
namzdf	ln_zdfgls=.true.	ln_zdfevd=.true. rn_avevd=60. rn_avm0=1.2e-6 rn_avt0=1.2e-6
namzdf_gls	rn_emin=1.e-7 rn_epsmin=1.e-12 ln_length_lim=.true. rn_clim_galp=0.53 ln_sigpsi=.true. rn_crban=100. rn_charn=100000.0 rn_hsro=0.003 rn_frac_hs=1.3 nn_z0_met=1 nn_bc_surf=0 nn_bc_bot=1 nn_stab_func=2 nn_clos=1	

Table S2. Summary of WAVEWATCH III compilation switches, descriptions of key physical parameterisations and numerical options applied in the wave model setup.

Switch	**Summary description**
ST4	Source term package for wave growth & dissipation (Ardhuin et al. 2010)
SMC	Activate SMC grid
FLX0	No separate flux routine; fluxes computed within source terms
LN1	Linear wave growth at low wind speeds (Cavaleri & Rizzoli 1981)
NL1	Discrete interaction approximation (DIA; Hasselmann et al. 1985)
BT1	JONSWAP bottom friction formulation (Hasselmann et al. 1973)
DB1	Depth-induced breaking (Battjes & Janssen 1978)
PR2	Higher-order dispersion correction via the classical GSE alleviation method
UNO	Second-order UNO propagation scheme
WNT1	Linear interpolation of wind over time
WNX1	Approximate linear interpolation of wind over space
RWND	Correct wind speed for current velocity
CRT1	Linear interpolation of current over time
CRX1	Approximate linear interpolation of current over space
SHRD	Shared memory model
NOGRB	No GRIB package included
WNT0	No linear interpolation of wind (Coupled mode)
CRT0	No linear interpolation of current (Coupled mode)

Table S3. Monthly performance statistics for significant wave height (H_s) from the standalone cSINGV_W simulation against satellite-altimeter observations over the full model domain during January–June 2019. N denotes the number of observation–model pairs; SI denotes the scatter index; and KS denotes the Kolmogorov–Smirnov statistic.

Month	N	Bias (m)	RMSE (m)	SI	Correlation	KS score
January	21892	-0.018	0.200	0.150	0.930	0.037
February	13043	-0.018	0.179	0.192	0.910	0.109
March	11073	-0.067	0.214	0.234	0.918	0.220
April	11572	-0.195	0.287	0.270	0.953	0.313
May	14671	-0.118	0.236	0.227	0.944	0.228
June	20290	-0.123	0.249	0.185	0.966	0.127

Table S4. Same as Table S3, but for the fully coupled cSINGV simulation.

Month	N	Bias (m)	RMSE (m)	SI	Correlation	KS score
January	21892	-0.050	0.203	0.152	0.931	0.050
February	13043	-0.025	0.175	0.188	0.913	0.111
March	11073	−0.079	0.211	0.231	0.920	0.218
April	11572	−0.194	0.283	0.267	0.954	0.311
May	14671	−0.119	0.228	0.220	0.950	0.222
June	20290	−0.139	0.251	0.187	0.969	0.132

Table S5. Computational requirements of the atmosphere-only cSINGV_A and fully coupled cSINGV configurations for one 24-h simulated forecast day. Allocated core-hours were calculated as the number of allocated CPU cores multiplied by the elapsed wall-clock time in hours.

Configuration	**Allocated cores**	**Wall-clock time per 24-h forecast day**	**Allocated core-hours per forecast day**
cSINGV_A	1,152	76 min	1,459
cSINGV	2,176	80 min	2,901

Table S6. Summary of cSINGV_W tuning for the wave growth parameter (bmax).

Expt. No.	**BETAMAX**	**Correlation**	**Bias**	**RMSE**	**SI**
1	1.0	0.97	-0.18	0.27	0.20
2	1.25	0.97	-0.14	0.25	0.18
3	1.39 (MO)	0.97	-0.12	0.25	0.18
4	1.43 (ECMWF)	0.97	-0.12	0.25	0.18
5	1.5	0.97	-0.11	0.25	0.18
6	1.75	0.97	-0.08	0.24	0.18
7	2.0	0.96	-0.06	0.25	0.18

Table S7. Summary of cSINGV_W tuning for the shallow water physics.

Expt. No.	**Correlation**	**Bias**	**RMSE**	**SI**
8	0.94	+0.06	0.31	0.23
9	0.97	-0.18	0.27	0.20
10	0.97	-0.08	0.24	0.18
11	0.97	-0.19	0.28	0.20
12	0.97	-0.21	0.29	0.21
13	0.97	-0.19	0.28	0.20

Table S8. Final wave-growth and swell-dissipation parameters specified in the SIN4 namelist.

Parameter	**Final value**
BETAMAX	1.75
SWELLF	0.66
TAUWSHELTER	0.30
SWELLF3	0.022
SWELLF4	115000.0
SWELLF7	432000.0